Possible two-component spin-singlet pairings in Sr_2RuO_4

San-Jun Zhang,[1] Da Wang,[1,2,*] and Qiang-Hua Wang[1,2,†]
[1]*National Laboratory of Solid State Microstructures and School of Physics, Nanjing University, Nanjing 210093, China*
[2]*Collaborative Innovation Center of Advanced Microstructures, Nanjing University, Nanjing 210093, China*

(Received 21 April 2021; revised 19 August 2021; accepted 24 August 2021; published 3 September 2021)

Recent experiments suggest a multicomponent pairing function in Sr_2RuO_4, which appears to be inconsistent with the absence of an apparent cusp in the transition temperature T_c as a function of the uniaxial strain. We show, however, that the theoretical cusp in T_c for a multicomponent pairing can be easily smeared out by the spatial inhomogeneity of strain, and the experimental data can be reproduced qualitatively by a percolation model. These results shed light on multicomponent pairings. We then perform a thorough group-theoretical classification of the pairing functions, taking the spin-orbit coupling into account. We list all 13 types of two-component spin-singlet pairing functions, with 8 of them belonging to the E_g representation. In particular, we find two types of intraorbital pairings in the E_g representation (k_xk_z, k_yk_z) are favorable in view of most existing experiments.

DOI: 10.1103/PhysRevB.104.094504

I. INTRODUCTION

Sr_2RuO_4 is a layered perovskite superconductor isostructural to the cuprate La_2CuO_4 and has been widely studied since its discovery [1]. Muon spin rotation (μSR) [2,3] and Kerr experiments [4] indicate the time-reversal symmetry is spontaneously broken in the superconducting state, suggesting that the pairing order parameter must have multiple components. This is, indeed, consistent with ultrasound experiments [5,6]. Theoretically, a symmetry-protected multicomponent pairing function must belong to the twofold-degenerate E_g or E_u representation of the underlying D_{4h} point group of Sr_2RuO_4. The two types of pairing functions differ in parity. Early phase-sensitive probes [7–11] suggest the pairing function transforms as $k_x + ik_y$, belonging to the E_u representation, as proposed in the early stage [12,13].

However, more recent and refined experiments strongly challenge the $k_x + ik_y$ spin-triplet pairing. First, according to the Ginzburg-Landau (GL) theory, the two components of the order parameter in the E_u (or even E_g) representation can couple to the uniaxial strain linearly, leading to a cusplike feature in the superconducting transition temperature T_c as a function of the uniaxial strain. But no apparent cusp is observed experimentally [14–17], and this appears to rule out the possibility of a multicomponent order parameter. Second, if the pairing is spin triplet, the Knight shift should not drop below T_c (at least for a magnetic field applied orthogonal to the so-called d vector of the triplet). But it actually drops significantly in strained as well as unstrained samples in most recent and refined nuclear magnetic resonance (NMR) experiments [18,19]. These NMR experiments and the polarized neutron experiment [20] act strongly against spin-triplet pairing, making it difficult to reconcile with phase-sensitive experiments [21]. Importantly, in the same type of samples the ultrasonic measurement reveals the signature of a multicomponent order parameter [5,6]. On the one hand, it combines the behavior of the Knight shift, suggesting spin-singlet pairing that transforms as the E_g or even E_u representation in the presence of spin-orbital coupling (SOC), but on the other hand, it seems to conflict with the absence of a cusp in T_c versus the uniaxial strain [14–17]. The current situation is therefore rather paradoxical and motivates careful reexamination of the pairing symmetry in Sr_2RuO_4 [22–28] regarding issues such as single component vs multicomponent, spin singlet vs triplet, nodal vs nodeless quasiparticles, etc.

In this work, we try to reconcile the paradox and reinforce the possibility of the spin-singlet pairing in the degenerate E_g representation. First, we realize that the strain in the reported sample is inhomogeneous, as seen in a scanning superconducting quantum interference device (SQUID) experiment [17]. We show with a percolation model that in the presence of an inhomogeneous background of strain, the cusp is absent or smeared out even if the pairing function is in the E_g or E_u representation. Combining the ultrasound, Knight-shift, neutron, μSR, and Kerr experiments provides a consistent picture of multicomponent pairing in the E_g or E_u representation. Since various forms of E_g and E_u representations remain in the system with multiple orbitals and SOC, we perform a thorough group-theoretical classification of the pairing functions in spin, orbital, and momentum spaces and discuss the relevance of various pairing functions in view of the other experiments, such as superfluid density [29], specific heat [30,31], and thermal transports [32,33]. We find two types of intraorbital pairings in the E_g representation (transforming as $k_xk_z + ik_yk_z$) are the most favorable in view of such experiments.

II. STRAIN EFFECT

We first discuss the impact of the recent experiments using strain as the tuning parameter. The uniaxial component of the strain, $\varepsilon = \epsilon_{xx} - \epsilon_{yy}$, where ϵ_{ab} is the element of the

*dawang@nju.edu.cn
†qhwang@nju.edu.cn

strain tensor, transforms as B_{1g} under symmetry operations. Since Sr_2RuO_4 is D_{4h} symmetric, the multicomponent pairing order parameter must belong to the E_g or E_u representation, except for accidental degeneracy between one-dimensional representations [28] (which will not interest us here). Let the two-component order parameter be (η_1, η_2), which transforms as (x, y) in the E_u case and (xz, yz) in the E_g case. In either case, it is clear that $|\eta_1|^2 - |\eta_2|^2$ also transforms as B_{1g}. Therefore, the order parameters can couple to ε linearly as $\alpha\varepsilon(|\eta_1|^2 - |\eta_2|^2)$, with a coefficient α. Within the GL theory, this coupling lifts the degeneracy in the bare transition temperatures for the two components, and the modified transition temperature is the higher one, so that the change in T_c behaves as $\delta T_c \propto |\varepsilon|$, resulting in a cusp dependence in ε [14,28]. Rather unexpectedly, no apparent cusp feature has been observed in strain experiments [14–17]. This result appears to rule out the picture of multicomponent order parameter in Sr_2RuO_4, provided that the strain distribution is uniform in the sample. In the literature, two possibilities have been proposed towards reconciling this paradox: fluctuation-induced first-order phase transition [34,35] and T_c determined by a critical pairing amplitude [36].

However, the recent scanning SQUID experiment [17] showed that the local T_c, measured in different regions of the sample, reaches the minimum at different values of ε, although the minimal T_c itself is only slightly changed. This fact may imply inhomogeneity of the strain distribution except for the possibility of sample slipping in the experiment [17]. To investigate the effect of such inhomogeneity, we assume a background strain $\varepsilon_{\rm loc}$, which distributes over the sample statistically with a probability density $\rho(\varepsilon_{\rm loc})$. The total strain at a specific spatial point is given by $\varepsilon_{\rm eff} = \varepsilon + \varepsilon_{\rm loc}$, where ε represents the applied (external) strain in experiments. It defines a local bare transition temperature $\tau(\varepsilon_{\rm eff}) = T_{c0} + |\alpha\varepsilon_{\rm eff}|$, where T_{c0} is the value of T_c in the absence of any strain. We then have to deal with a system with T_c inhomogeneity arising from the strain distribution. Notice that experimentally, the position-dependent T_c is determined by measuring the diamagnetic susceptibility within a ring of diameter $\sim$2 μm [17], which is much larger than the superconducting coherence length $\xi < 100$ nm [13]. Therefore, the superfluid-induced diamagnetic signal can be established only if the associated large area has entered the superconducting state collectively. The large area justifies a statistical treatment of the strain distribution. Using the simplest percolation model, we assume that superconductivity is achieved below T_c if the statistical probability for $\tau(\varepsilon_{\rm eff}) > T_c$ is above a percolation threshold p_c. In the classical percolation model, it is known that $p_c = 1$ in one dimension, $p_c = 0.5$ in two dimensions, and p_c is lower in higher dimensions. In our case it is reasonable to speculate that $0 < p_c < 0.5$, but its exact value is unimportant for qualitative purposes. In this picture, we can determine $\delta T_c = T_c - T_{c0}$ implicitly as

$$\int \theta(\alpha|\varepsilon + \varepsilon_{\rm loc}| - \delta T_c)\rho(\varepsilon_{\rm loc})d\varepsilon_{\rm loc} = p_c, \qquad (1)$$

where θ is the Heaviside step function. It turns out that the resulting δT_c no longer develops a cusp in the applied ε as long as $p_c > 0$. To see this point most straightforwardly, we can take the derivative with respect to ε in Eq. (1) to obtain

$$\frac{\partial\delta T_c}{\partial\varepsilon}\left[\rho\left(-\varepsilon + \frac{\delta T_c}{\alpha}\right) + \rho\left(-\varepsilon - \frac{\delta T_c}{\alpha}\right)\right] = \alpha\left[\rho\left(-\varepsilon + \frac{\delta T_c}{\alpha}\right) - \rho\left(-\varepsilon - \frac{\delta T_c}{\alpha}\right)\right]. \qquad (2)$$

Clearly, $\partial\delta T_c/\partial\varepsilon = 0$ at $\varepsilon = 0$ as long as $\rho(\varepsilon_{\rm loc})$ is an even function. As a specific model, we assume a Gaussian distribution, $\rho(\varepsilon_{\rm loc}) = \frac{1}{\sqrt{2\pi}\sigma}e^{-\varepsilon_{\rm loc}^2/2\sigma^2}$. Then Eq. (1) can be integrated out exactly, yielding

$$\mathrm{erf}\left(\frac{\delta T_c - \alpha\varepsilon}{\sqrt{2}\sigma\alpha}\right) + \mathrm{erf}\left(\frac{\delta T_c + \alpha\varepsilon}{\sqrt{2}\sigma\alpha}\right) = 2(1 - p_c), \qquad (3)$$

where erf is the standard error function. In Fig. 1, we plot δT_c vs ε for various choices of p_c. It can be seen that δT_c depends smoothly on ε unless the strain distribution width σ goes to zero (uniform strain distribution). Therefore, we have shown that the smooth dependence of T_c on small ε cannot rule out the possibility of multicomponent order parameter in Sr_2RuO_4. Instead, combining the strain experiments with the μSR [2,3], neutron [20], Kerr [4], and ultrasound [5,6] experiments actually provides a consistent picture of spin-singlet pairing in the E_g or E_u representation.

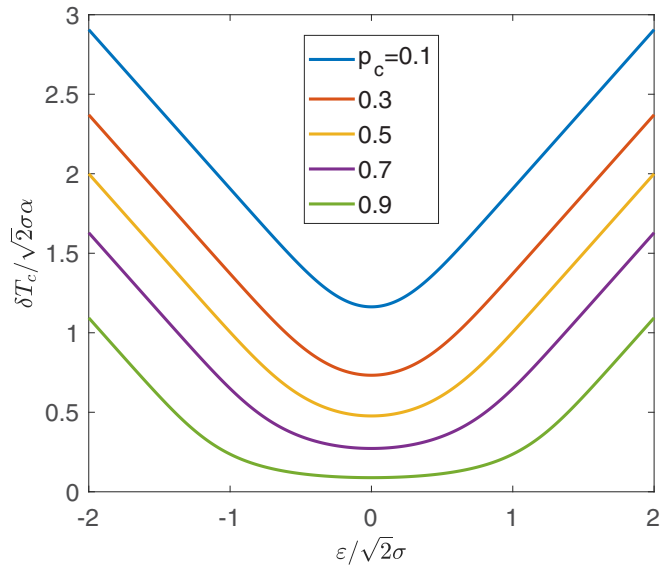

FIG. 1. δT_c vs uniaxial strain ε at different percolation thresholds p_c. σ is the standard deviation of the Gaussian distribution $\rho(\varepsilon_{\rm loc})$.

We make the following remarks: (1) Experimentally, T_c in different regions reaches the minimum at different applied strains. This behavior can be explained if the applied strain itself is nonuniform in the sample, such that the strain distribution is biased differently at different spatial regions (which are microscopically large but macroscopically small on the scale of coherence length). (2) The approximation of linear coupling to strain is valid only at small strains. Larger strains may modify the electronic structure significantly (because the Fermi level is close to the Van Hove singularity in the γ band), and the effect inevitably goes beyond the linear approximation and beyond the scope of this work.

III. GROUP CLASSIFICATION

Sr_2RuO_4 is a multiorbital system, and its low-energy bands are dominantly described by three t_{2g} orbitals (d_{xz}, d_{yz}, d_{xy}) [13]. On the other hand, angle-resolved photoemission spectroscopy has shown its band structures are strongly affected by the SOC effect [37,38]. Therefore, a thorough group classification of the possible pairing functions is needed, taking into account the t_{2g} orbitals, the atomic SOC, and the D_{4h} group. There has been some progress along this direction [22–28], and our strategy mainly follows Ref. [23]. A general pairing Hamiltonian for electrons at momenta $\mathbf{k}$ and $-\mathbf{k}$ can be written as $\psi^\dagger_{\mathbf{k}}\Delta(\mathbf{k})i\sigma_2\psi^{\dagger,t}_{-\mathbf{k}}+\text{H.c.}$, where $\psi_{\mathbf{k}}$ is a multicomponent spinor composed of electron annihilation operators of all internal degrees of freedom, such as orbital and spin, $\Delta(\mathbf{k})$ is a matrix function in the orbital and spin bases, and $\sigma_{\mu=0,1,2,3}$ will henceforth denote the identity and Pauli matrices acting on spins. Under a group operation $g\in D_{4h}$, the spinor transforms as $\psi'_{\mathbf{k}}=U_g\psi_{g^{-1}\mathbf{k}}$, where U_g encodes the $\mathbf{k}$-independent transformation on orbitals and spins. Correspondingly, the pairing matrix transforms as $\Delta'_{\mathbf{k}}=U_g\Delta_{g^{-1}\mathbf{k}}U_g^\dagger$, where we used the fact that $U_g=TU_gT^{-1}$ for transformation on spins and on real orbital bases, with $T=i\sigma_2\mathcal{K}$ being the time-reversal operator (and $\mathcal{K}$ being the complex conjugation operator). The pairing matrix can be written as a linear superposition of the tensor products $\Lambda_o\otimes\Lambda_s\otimes f_{\mathbf{k}}$, where $\Lambda_{o(s)}$ is a matrix describing a fermion bilinear operator superposition in the orbital (spin) basis and $f_{\mathbf{k}}$ is a function of $\mathbf{k}$. To set up notations, we define $\lambda_{(ab)}$ as a self-explaining matrix in the orbital basis (d_{xz}, d_{yz}, d_{xy}) such that its elements read $\lambda^{ij}_{(ab)}=\delta_{ia}\delta_{jb}$. Such matrices can be used to expand Λ_o and form irreducible representations. For example, $\lambda_{(11)}+\lambda_{(22)}\sim A_{1g}$, $\lambda_{(11)}-\lambda_{(22)}\sim B_{1g}$, etc. The matrix Λ_s is expanded by σ_μ, with σ_0 ($\sigma_{1,2,3}$) representing the spin-singlet (spin-triplet) component(s). Under D_{4h} these matrices transform as $\sigma_0\sim A_{1g}$, $\sigma_3\sim A_{2g}$, and $(\sigma_1,\sigma_2)\sim E_g$. (Note that under time reversal, σ_0 is invariant, while $\sigma_{1,2,3}$ changes sign.) The classification of the function $f_{\mathbf{k}}$ is standard. The details of the separate classifications are presented in Appendix A. Finally, the entire pairing function is classified by decomposing the tensor products of the separate irreducible representations. The complete results are also presented in Appendix A. Note that it is possible that multiple pairing functions with either a spin singlet or triplet transform identically as the same irreducible representation. Such pairing functions could mix, but this does not mean they have to since the extent of mixing of such pairing functions is not dictated by symmetry alone.

TABLE I. Spin-singlet pairing functions in the E_g and E_u representations. Here $\lambda_{(ab)}$ denotes a matrix in the orbital basis, with the elements $\lambda^{ij}_{(ab)}=\delta_{ia}\delta_{jb}$. In each row, the two basis functions transform as (xz, yz) in the E_g representation and as (x, y) in the E_u representation. The identity matrix σ_0 in the spin basis for spin-singlet pairing is omitted for brevity.

	Pairing	xz or x	yz or y
E_g	1	$\lambda_{(23)}+\lambda_{(32)}$	$\lambda_{(13)}+\lambda_{(31)}$
	2	$k_xk_y(k_x^2-k_y^2)(\lambda_{(13)}+\lambda_{(31)})$	$-k_xk_y(k_x^2-k_y^2)(\lambda_{(23)}+\lambda_{(32)})$
	3	$(k_x^2-k_y^2)(\lambda_{(23)}+\lambda_{(32)})$	$-(k_x^2-k_y^2)(\lambda_{(13)}+\lambda_{(31)})$
	4	$k_xk_y(\lambda_{(13)}+\lambda_{(31)})$	$k_xk_y(\lambda_{(23)}+\lambda_{(32)})$
	5	$k_xk_z(\lambda_{(11)}+\lambda_{(22)})$	$k_yk_z(\lambda_{(11)}+\lambda_{(22)})$
	6	$k_yk_z(\lambda_{(12)}+\lambda_{(21)})$	$k_xk_z(\lambda_{(12)}+\lambda_{(21)})$
	7	$k_xk_z\lambda_{(33)}$	$k_yk_z\lambda_{(33)}$
	8	$k_xk_z(\lambda_{(11)}-\lambda_{(22)})$	$-k_yk_z(\lambda_{(11)}-\lambda_{(22)})$
E_u	9	$k_xk_yk_z(k_x^2-k_y^2)(\lambda_{(13)}-\lambda_{(31)})$	$k_xk_yk_z(k_x^2-k_y^2)(\lambda_{(23)}-\lambda_{(32)})$
	10	$k_z(\lambda_{(23)}-\lambda_{(32)})$	$k_z(\lambda_{(13)}-\lambda_{(31)})$
	11	$k_xk_yk_z(\lambda_{(13)}-\lambda_{(31)})$	$k_xk_yk_z(\lambda_{(13)}-\lambda_{(31)})$
	12	$k_z(k_x^2-k_y^2)(\lambda_{(23)}-\lambda_{(32)})$	$k_z(k_x^2-k_y^2)(\lambda_{(13)}-\lambda_{(31)})$
	13	$k_y(\lambda_{(12)}-\lambda_{(21)})$	$k_x(\lambda_{(12)}-\lambda_{(21)})$

Here we focus on spin-singlet E_g and E_u representations, along the lines of the previous discussions of the experiments. Such pairing functions are listed in Table I. Note that if necessary, each pairing function could be multiplied by an additional A_{1g} factor function of $\mathbf{k}$ to describe pairing on longer bonds. There are eight pairing functions in the E_g representation and five in the E_u representation. (Note that E_u spin singlet is allowed if the pairing function is odd under orbital exchange.) Among these pairing functions, only three of them (5, 7, and 8) in the E_g representation have intraorbital pairing, while all the others involve interorbital pairing. If the pairing arises from electron-electron correlations, the orbital-wise matrix element effect in the overlap between Bloch states should render interorbital pairing less relevant. In this case, we may speculate that the above three E_g pairing functions are the most important. Once the dominant pairing functions in the E_g representation are realized, the others in the same representation may be induced by subleading correlation effects, so for sufficient generality, we include all of the E_g functions in the list. In this setting, we can write the two degenerate general pairing functions in the E_g representation explicitly as, in the orbital basis,

$$\Delta_{xz}(\mathbf{k})=\begin{bmatrix}(d_5+d_8)k_xk_z & d_6k_yk_z & d_4k_xk_y+d_2k_xk_y\left(k_x^2-k_y^2\right)\\ d_6k_yk_z & (d_5-d_8)k_xk_z & d_3\left(k_x^2-k_y^2\right)+d_1\\ d_4k_xk_y+d_2k_xk_y\left(k_x^2-k_y^2\right) & d_3\left(k_x^2-k_y^2\right)+d_1 & d_7k_xk_z\end{bmatrix},$$

$$\Delta_{yz}(\mathbf{k})=\begin{bmatrix}(d_5-d_8)k_yk_z & d_6k_xk_z & -d_3\left(k_x^2-k_y^2\right)+d_1\\ d_6k_xk_z & (d_5+d_8)k_yk_z & d_4k_xk_y-d_2k_xk_y\left(k_x^2-k_y^2\right)\\ -d_3\left(k_x^2-k_y^2\right)+d_1 & d_4k_xk_y-d_2k_xk_y\left(k_x^2-k_y^2\right) & d_7k_yk_z\end{bmatrix}. \quad (4)$$

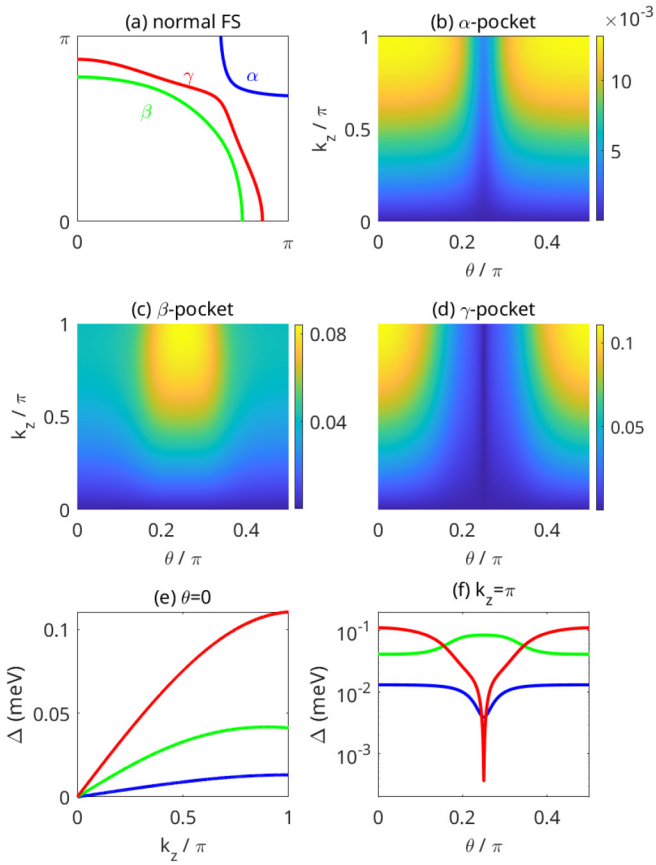

FIG. 2. A possible pairing of E_g with $d_7 = 0.01$ and $d_8 = 0.005$ (in mRy). The normal state FS at $k_z = 0$ is plotted in (a) to define the α, β, and γ pockets. In (b) to (d), the quasiparticle gaps are plotted on the (θ, k_z) plane for each pocket. θ is defined as the azimuth angle relative to the center of each pocket. The k_z dependence at $\theta = 0$ is explicitly shown in (e), and θ dependence at $k_z = \pi$ is shown in (f).

Here $d_{1\sim8}$ are coefficients multiplying the respective E_g functions in Table I. The relative ratios among these coefficients depend on the microscopic details. (Once the relative ratio is fixed, in the GL theory, the global coefficients act as order parameters and carry or transform as the same E_g representation.) Below the transition temperature, it is usually favorable for the two degenerate pairing functions, $\Delta_{xz}(\mathbf{k})$ and $\Delta_{yz}(\mathbf{k})$, to combine into the time-reversal symmetry-breaking form, $\Delta(\mathbf{k}) = \Delta_{xz}(\mathbf{k}) \pm i\Delta_{yz}(\mathbf{k})$ to maximize the pairing gaps on the Fermi surface and gain energy.

IV. GAP STRUCTURE

We now discuss the quasiparticle excitations subject to the above spin-singlet E_g pairing functions. The Bogoliubov–de Gennes Hamiltonian in the Nambu basis $\Psi_{\mathbf{k}}^\dagger = (\psi_{\mathbf{k}}^\dagger, -\psi_{-\mathbf{k}}^t i\sigma_2)$ is

$$H = \sum_{\mathbf{k}} \Psi_{\mathbf{k}}^\dagger \begin{bmatrix} h_{\mathbf{k}} & \Delta(\mathbf{k}) \\ \Delta^\dagger(\mathbf{k}) & -T h_{-\mathbf{k}} T^{-1} \end{bmatrix} \Psi_{\mathbf{k}}, \tag{5}$$

where $h_{\mathbf{k}}$ is the normal state single-particle Hamiltonian taken from Refs. [37,39] with atomic SOC and

TABLE II. Irreducible representations of the pairing matrix in orbital, spin, and momentum spaces. The total pairing can be any tensor product of these three parts with odd parity in total.

	Orbital	Spin	$f(k)$
A_{1g}	$\lambda_{(11)} + \lambda_{(22)}$ $\lambda_{(33)}$	σ_0	1
A_{2g}	$\lambda_{(12)} - \lambda_{(21)}$	σ_3	$k_x k_y (k_x^2 - k_y^2)$
B_{1g}	$\lambda_{(11)} - \lambda_{(22)}$		$k_x^2 - k_y^2$
B_{2g}	$\lambda_{(12)} + \lambda_{(21)}$		$k_x k_y$
E_g	$(\lambda_{(13)} + \lambda_{(31)}, \lambda_{(23)} + \lambda_{(32)})$, $(\lambda_{(13)} - \lambda_{(31)}, \lambda_{(23)} - \lambda_{(32)})$	(σ_1, σ_2)	$(k_x k_z, k_y k_z)$
A_{1u}			$k_x k_y k_z (k_x^2 - k_y^2)$
A_{2u}			k_z
B_{1u}			$k_x k_y k_z$
B_{2u}			$k_z (k_x^2 - k_y^2)$
E_u			(k_x, k_y)

$\Delta(\mathbf{k}) = \Delta_{xz}(\mathbf{k}) + i\Delta_{yz}(\mathbf{k})$ (tensor produced implicitly by σ_0). In order to obtain the desired $(k_x k_z, k_y k_z)$ intraorbital pairing as discussed above, we consider the nearest-neighbor interlayer pairings on bonds $(\pm a/2, \pm a/2, \pm c/2)$, where a and c are in-plane and out-of-plane lattice constants. The simple form factor $f_{\mathbf{k}}$ is replaced by the corresponding lattice harmonics, e.g., $k_x k_z \to \sin(k_x a/2)\sin(k_z c/2)$, $k_x^2 - k_y^2 \to \cos(k_x a/2) - \cos(k_y a/2)$, etc. The quasiparticle gaps for different pairings, characterized by the coefficients $d_{i=1,2,\ldots,8}$, can be found in Appendix B. For all the E_g pairings, there is a horizontal nodal line at $k_z = 0$ by symmetry. It is consistent with the specific heat [31] and neutron [40] experiments. When interorbital pairing is included, the horizontal nodal line may expand into a nodal torus, forming the Bogoliubov Fermi surface [41], as shown in Appendix B. This would generate a finite zero-energy quasiparticle density of states, which is, however, inconsistent with the universal thermal conductivity [32,33], which can arise only if the energy gap is nodal or quasinodal [42–44] or the Bogoliubov Fermi surface is too small [45]. Furthermore, the substantial nonzero c-axis thermal conductivity in the $T = 0$ K limit [33] was taken to be strong evidence to rule out the "simple" $k_z = 0$ horizontal nodal line picture. Recently, a scanning tunneling microscopy experiment [46] also indicated the existence of a vertical nodal line (or gap minima) along the (11) direction. Taking these discussions together, we find (d_7, d_8) pairing may be the most relevant. With the parametrization $d_7 = 2d_8 = 0.01$ mRy, the quasiparticle gaps on the three pockets defined in Fig. 2(a) are plotted on the (θ, k_z) plane in Figs. 2(b) to 2(d), where θ is the azimuthal angle relative to the pocket center. In particular, for clarity, the gaps along two cuts, $\theta = 0$ and $k_z = \pi$, are given in Figs. 2(e) and 2(f). Clearly, in addition to the horizontal nodal lines for all three pockets, there is a very deep gap minimum at $\theta = \pi/4$ on the γ pocket. This quasinode stems from the effect of SOC, which causes the Bloch state at the Fermi angle $\theta = \pi/4$ on the γ pocket to be dominated by the d_{xz} and d_{yz} components, while the pairing of the latter two orbitals $(\lambda_{(11)} - \lambda_{(22)}$ contributes a B_{1g} factor within the E_g representation) has an exact node at $\theta = \pi/4$. This

TABLE III. Full classification of Sr_2RuO_4. In general, a pairing can be written as a linear superposition of the tensor products $\lambda_{(ab)} \otimes \sigma_\mu \otimes f_{\mathbf{k}}$. Notice that $f_{\mathbf{k}}$ give only the lowest-order lattice harmonics. For compactness, we use the notation λ_{ab} to represent the matrix $\lambda_{(ab)}$ as defined in the main text.

Irreducible representation	σ_0	σ_3	(σ_1, σ_2)
A_{1g}	$\lambda_{11}+\lambda_{22}$ λ_{33} $(k_x^2-k_y^2)(\lambda_{11}-\lambda_{22})$ $k_xk_y(\lambda_{12}+\lambda_{21})$ $k_yk_z(\lambda_{13}+\lambda_{31})+k_xk_z(\lambda_{23}+\lambda_{32})$	$(\lambda_{12}-\lambda_{21})\sigma_3$ $[k_xk_z(\lambda_{13}-\lambda_{31})-k_yk_z(\lambda_{23}-\lambda_{32})]\sigma_3$	$(\lambda_{12}-\lambda_{21})(k_xk_z\sigma_1-k_yk_z\sigma_2)$ $(\lambda_{13}-\lambda_{31})\sigma_1+(\lambda_{23}-\lambda_{32})\sigma_2$ $k_xk_y(k_x^2-k_y^2)[(\lambda_{13}-\lambda_{31})\sigma_2-(\lambda_{23}-\lambda_{32})\sigma_1]$ $(k_x^2-k_y^2)[(\lambda_{13}-\lambda_{31})\sigma_1-(\lambda_{23}-\lambda_{32})\sigma_2]$ $k_xk_y[(\lambda_{13}-\lambda_{31})\sigma_2+(\lambda_{23}-\lambda_{32})\sigma_1]$
A_{2g}	$k_xk_y(k_x^2-k_y^2)(\lambda_{11}+\lambda_{22})$ $k_xk_y(k_x^2-k_y^2)\lambda_{33}$ $k_xk_y(\lambda_{11}-\lambda_{22})$ $(k_x^2-k_y^2)(\lambda_{12}+\lambda_{21})$ $k_xk_z(\lambda_{13}+\lambda_{31})-k_yk_z(\lambda_{23}+\lambda_{32})$	$k_xk_y(k_x^2-k_y^2)(\lambda_{12}-\lambda_{21})\sigma_3$ $[k_yk_z(\lambda_{13}-\lambda_{31})+k_xk_z(\lambda_{23}-\lambda_{32})]\sigma_3$	$(\lambda_{12}-\lambda_{21})(k_yk_z\sigma_1+k_xk_z\sigma_2)$ $(\lambda_{13}-\lambda_{31})\sigma_2-(\lambda_{23}-\lambda_{32})\sigma_1$ $k_xk_y(k_x^2-k_y^2)[(\lambda_{13}-\lambda_{31})\sigma_1+(\lambda_{23}-\lambda_{32})\sigma_2]$ $(k_x^2-k_y^2)[(\lambda_{13}-\lambda_{31})\sigma_2+(\lambda_{23}-\lambda_{32})\sigma_1]$ $k_xk_y[(\lambda_{13}-\lambda_{31})\sigma_1-(\lambda_{23}-\lambda_{32})\sigma_2]$
B_{1g}	$(k_x^2-k_y^2)(\lambda_{11}+\lambda_{22})$ $(k_x^2-k_y^2)\lambda_{33}$ $\lambda_{11}-\lambda_{22}$ $k_xk_y(k_x^2-k_y^2)(\lambda_{12}+\lambda_{21})$ $k_yk_z(\lambda_{13}+\lambda_{31})-k_xk_z(\lambda_{23}+\lambda_{32})$	$(k_x^2-k_y^2)(\lambda_{12}-\lambda_{21})\sigma_3$ $[k_xk_z(\lambda_{13}-\lambda_{31})+k_yk_z(\lambda_{23}-\lambda_{32})]\sigma_3$	$k_xk_z(\lambda_{12}-\lambda_{21})\sigma_1+k_yk_z(\lambda_{12}-\lambda_{21})\sigma_2$ $(\lambda_{13}-\lambda_{31})\sigma_1-(\lambda_{23}-\lambda_{32})\sigma_2$ $k_xk_y(k_x^2-k_y^2)[(\lambda_{13}-\lambda_{31})\sigma_2+(\lambda_{23}-\lambda_{32})\sigma_1]$ $(k_x^2-k_y^2)[(\lambda_{13}-\lambda_{31})\sigma_1+(\lambda_{23}-\lambda_{32})\sigma_2]$ $k_xk_y[(\lambda_{13}-\lambda_{31})\sigma_2-(\lambda_{23}-\lambda_{32})\sigma_1]$
B_{2g}	$k_xk_y(\lambda_{11}+\lambda_{22})$ $k_xk_y\lambda_{33}$ $k_xk_y(k_x^2-k_y^2)(\lambda_{11}-\lambda_{22})$ $\lambda_{12}+\lambda_{21}$ $k_xk_z(\lambda_{13}+\lambda_{31})-k_yk_z(\lambda_{23}+\lambda_{32})$	$k_xk_y(\lambda_{12}-\lambda_{21})\sigma_3$ $[k_yk_z(\lambda_{13}-\lambda_{31})-k_xk_z(\lambda_{23}-\lambda_{32})]\sigma_3$	$(\lambda_{12}-\lambda_{21})(k_yk_z\sigma_1-k_xk_z\sigma_2)$ $(\lambda_{13}-\lambda_{31})\sigma_2+(\lambda_{23}-\lambda_{32})\sigma_1$ $k_xk_y(k_x^2-k_y^2)[(\lambda_{13}-\lambda_{31})\sigma_1-(\lambda_{23}-\lambda_{32})\sigma_2]$ $(k_x^2-k_y^2)[(\lambda_{13}-\lambda_{31})\sigma_2-(\lambda_{23}-\lambda_{32})\sigma_1]$ $k_xk_y[(\lambda_{13}-\lambda_{31})\sigma_1+(\lambda_{23}-\lambda_{32})\sigma_2]$
E_g	$k_z(k_x,k_y)(\lambda_{11}+\lambda_{22})$ $k_z(k_x,k_y)\lambda_{33}$ $k_z(k_x,-k_y)(\lambda_{11}-\lambda_{22})$ $k_z(k_y,k_x)(\lambda_{12}+\lambda_{21})$ $(\lambda_{23}+\lambda_{32},\lambda_{13}+\lambda_{31})$ $k_xk_y(k_x^2-k_y^2)[\lambda_{13}+\lambda_{31},-(\lambda_{23}+\lambda_{32})]$ $(k_x^2-k_y^2)[\lambda_{23}+\lambda_{32},-(\lambda_{23}+\lambda_{32})]$ $k_xk_y(\lambda_{13}+\lambda_{31},\lambda_{23}+\lambda_{32})$	$k_z(k_x,k_y)(\lambda_{12}-\lambda_{21})\sigma_3$ $[\lambda_{13}-\lambda_{31},-(\lambda_{23}-\lambda_{32})]\sigma_3$ $k_xk_y(k_x^2-k_y^2)(\lambda_{23}-\lambda_{32},\lambda_{13}-\lambda_{31})\sigma_3$ $(k_x^2-k_y^2)(\lambda_{13}-\lambda_{31},\lambda_{23}-\lambda_{32})\sigma_3$ $k_xk_y[\lambda_{23}-\lambda_{32},-(\lambda_{13}-\lambda_{31})]\sigma_3$	$(\lambda_{12}-\lambda_{21})(\sigma_1,-\sigma_2)$ $k_xk_y(k_x^2-k_y^2)(\lambda_{12}-\lambda_{21})(\sigma_2,\sigma_1)$ $(k_x^2-k_y^2)(\lambda_{12}-\lambda_{21})(\sigma_1,\sigma_2)$ $k_xk_y(\lambda_{12}-\lambda_{21})(\sigma_2,-\sigma_1)$ $k_z(k_x,k_y)[(\lambda_{13}-\lambda_{31})\sigma_1+(\lambda_{23}-\lambda_{32})\sigma_2]$ $k_z(k_y,-k_x)[(\lambda_{13}-\lambda_{31})\sigma_2-(\lambda_{23}-\lambda_{32})\sigma_1]$ $k_z(k_x,-k_y)[(\lambda_{13}-\lambda_{31})\sigma_1-(\lambda_{23}-\lambda_{32})\sigma_2]$ $k_z(k_y,k_x)[(\lambda_{13}-\lambda_{31})\sigma_2+(\lambda_{23}-\lambda_{32})\sigma_1]$
A_{1u}	$k_z(\lambda_{12}-\lambda_{21})$ $k_x(\lambda_{13}-\lambda_{31})-k_y(\lambda_{23}-\lambda_{32})$	$k_z(\lambda_{11}+\lambda_{22})\sigma_3$ $k_z\lambda_{33}\sigma_3$ $k_z(k_x^2-k_y^2)(\lambda_{11}-\lambda_{22})\sigma_3$ $k_xk_yk_z(\lambda_{12}+\lambda_{21})\sigma_3$ $[k_y(\lambda_{13}+\lambda_{31})+k_x(\lambda_{23}+\lambda_{32})]\sigma_3$	$(\lambda_{11}+\lambda_{22})(k_x\sigma_1-k_y\sigma_2)$ $\lambda_{33}(k_x\sigma_1-k_y\sigma_2)$ $(\lambda_{11}-\lambda_{22})(k_x\sigma_1+k_y\sigma_2)$ $(\lambda_{12}+\lambda_{21})(k_y\sigma_1-k_x\sigma_2)$ $k_xk_yk_z(k_x^2-k_y^2)[(\lambda_{13}+\lambda_{31})\sigma_1+(\lambda_{23}+\lambda_{32})\sigma_2]$ $k_z[(\lambda_{13}+\lambda_{31})\sigma_2-(\lambda_{23}+\lambda_{32})\sigma_1]$ $k_xk_yk_z[(\lambda_{13}+\lambda_{31})\sigma_1-(\lambda_{23}+\lambda_{32})\sigma_2]$ $k_z(k_x^2-k_y^2)[(\lambda_{13}+\lambda_{31})\sigma_2+(\lambda_{23}+\lambda_{32})\sigma_1]$
A_{2u}	$k_xk_yk_z(k_x^2-k_y^2)(\lambda_{12}-\lambda_{21})$ $k_y(\lambda_{13}-\lambda_{31})+k_x(\lambda_{23}-\lambda_{32})$	$k_xk_yk_z(k_x^2-k_y^2)(\lambda_{11}+\lambda_{22})\sigma_3$ $k_xk_yk_z(k_x^2-k_y^2)\lambda_{33}\sigma_3$ $k_xk_yk_z(\lambda_{11}-\lambda_{22})\sigma_3$ $k_z(k_x^2-k_y^2)(\lambda_{12}+\lambda_{21})\sigma_3$ $[k_x(\lambda_{13}+\lambda_{31})-k_y(\lambda_{23}+\lambda_{32})]\sigma_3$	$(\lambda_{11}+\lambda_{22})(k_y\sigma_1+k_x\sigma_2)$ $k_y\lambda_{33}\sigma_1+k_x\lambda_{33}\sigma_2$ $(\lambda_{11}-\lambda_{22})(k_y\sigma_1-k_x\sigma_2)$ $(\lambda_{12}+\lambda_{21})(k_x\sigma_1+k_x\sigma_2)$ $k_xk_yk_z(k_x^2-k_y^2)[(\lambda_{13}+\lambda_{31})\sigma_2-(\lambda_{23}+\lambda_{32})\sigma_1]$ $k_z[(\lambda_{13}+\lambda_{31})\sigma_1+(\lambda_{23}+\lambda_{32})\sigma_2]$ $k_xk_yk_z[(\lambda_{13}+\lambda_{31})\sigma_2+(\lambda_{23}+\lambda_{32})\sigma_1]$ $k_z(k_x^2-k_y^2)[(\lambda_{13}+\lambda_{31})\sigma_1-(\lambda_{23}+\lambda_{32})\sigma_2]$
B_{1u}	$k_z(k_x^2-k_y^2)(\lambda_{12}-\lambda_{21})$ $k_x(\lambda_{13}-\lambda_{31})+k_y(\lambda_{23}-\lambda_{32})$	$k_z(k_x^2-k_y^2)(\lambda_{11}+\lambda_{22})\sigma_3$ $k_z(k_x^2-k_y^2)\lambda_{33}\sigma_3$ $k_z(\lambda_{11}-\lambda_{22})\sigma_3$ $k_xk_yk_z(k_x^2-k_y^2)(\lambda_{12}+\lambda_{21})\sigma_3$ $[k_y(\lambda_{13}+\lambda_{31})-k_x(\lambda_{23}+\lambda_{32})]\sigma_3$	$(\lambda_{11}+\lambda_{22})(k_x\sigma_1+k_y\sigma_2)$ $\lambda_{33}(k_x\sigma_1+k_y\sigma_2)$ $(\lambda_{11}-\lambda_{22})(k_x\sigma_1-k_y\sigma_2)$ $(\lambda_{12}+\lambda_{21})(k_y\sigma_1+k_x\sigma_2)$ $k_xk_yk_z[(\lambda_{13}+\lambda_{31})\sigma_1-(\lambda_{23}+\lambda_{32})\sigma_2]$ $k_z[(\lambda_{13}+\lambda_{31})\sigma_2+(\lambda_{23}+\lambda_{32})\sigma_1]$ $k_xk_yk_z[(\lambda_{13}+\lambda_{31})\sigma_1+(\lambda_{23}+\lambda_{32})\sigma_2]$ $k_z(k_x^2-k_y^2)[(\lambda_{13}+\lambda_{31})\sigma_2-(\lambda_{23}+\lambda_{32})\sigma_1]$

TABLE III. (*Continued*.)

Irreducible representation	σ_0	σ_3	(σ_1, σ_2)
B_{2u}	$k_x k_y k_z(\lambda_{12} - \lambda_{21})$ $k_y(\lambda_{13} - \lambda_{31}) - k_x(\lambda_{23} - \lambda_{32})$	$k_x k_y k_z(\lambda_{11} + \lambda_{22})\sigma_3$ $k_x k_y k_z \lambda_{33}\sigma_3$ $k_x k_y k_z(k_x^2 - k_y^2)(\lambda_{11} - \lambda_{22})\sigma_3$ $k_z(\lambda_{12} + \lambda_{21})\sigma_3$ $[k_x(\lambda_{13} + \lambda_{31}) + k_y(\lambda_{23} + \lambda_{32})]\sigma_3$	$(\lambda_{11} + \lambda_{22})(k_y\sigma_1 - k_x\sigma_2)$ $\lambda_{33}(k_y\sigma_1 - k_x\sigma_2)$ $(\lambda_{11} - \lambda_{22})(k_y\sigma_1 + k_x\sigma_2)$ $(\lambda_{12} + \lambda_{21})(k_x\sigma_1 - k_y\sigma_2)$ $k_x k_y k_z[(\lambda_{13} + \lambda_{31})\sigma_2 + (\lambda_{23} + \lambda_{32})\sigma_1]$ $k_z[(\lambda_{13} + \lambda_{31})\sigma_1 - (\lambda_{23} + \lambda_{32})\sigma_2]$ $k_x k_y k_z[(\lambda_{13} + \lambda_{31})\sigma_2 - (\lambda_{23} + \lambda_{32})\sigma_1]$ $k_z(k_x^2 - k_y^2)[(\lambda_{13} + \lambda_{31})\sigma_1 + (\lambda_{23} + \lambda_{32})\sigma_2]$
E_u	$(k_y, -k_x)(\lambda_{12} - \lambda_{21})$ $k_x k_y k_z(k_x^2 - k_y^2)[\lambda_{13} - \lambda_{31}, -(\lambda_{23} - \lambda_{32})]$ $k_z(\lambda_{23} - \lambda_{32}, \lambda_{13} - \lambda_{31})$ $k_x k_y k_z(\lambda_{13} - \lambda_{31}, \lambda_{23} - \lambda_{32})$ $k_z(k_x^2 - k_y^2)[\lambda_{23} - \lambda_{32}, -(\lambda_{13} - \lambda_{31})]$	$(k_y, -k_x)(\lambda_{11} + \lambda_{22})\sigma_3$ $(k_y, -k_x)\lambda_{33}\sigma_3$ $(k_y, k_x)(\lambda_{11} - \lambda_{22})$ $\sigma_3(k_x, -k_y)(\lambda_{12} + \lambda_{21})\sigma_3$ $k_x k_y k_z(k_x^2 - k_y^2)(\lambda_{23} + \lambda_{32}, \lambda_{13} + \lambda_{31})\sigma_3$ $k_z[\lambda_{13} + \lambda_{31}, -(\lambda_{23} + \lambda_{32})]\sigma_3$ $k_x k_y k_z[\lambda_{23} + \lambda_{32}, -(\lambda_{13} + \lambda_{31})]\sigma_3$ $k_z(k_x^2 - k_y^2)(\lambda_{13} + \lambda_{31}, \lambda_{23} + \lambda_{32})\sigma_3$	$k_x k_y k_z(k_x^2 - k_y^2)(\lambda_{11} + \lambda_{22})(\sigma_1, -\sigma_2)$ $k_z(\lambda_{11} + \lambda_{22})(\sigma_2, \sigma_1)$ $k_x k_y k_z(\lambda_{11} + \lambda_{22})(\sigma_1, \sigma_2)$ $k_z(k_x^2 - k_y^2)(\lambda_{11} + \lambda_{22})(\sigma_2, -\sigma_1)$ $k_x k_y k_z(k_x^2 - k_y^2)\lambda_{33}(\sigma_1, -\sigma_2)$ $k_z\lambda_{33}(\sigma_2, \sigma_1)$ $k_x k_y k_z\lambda_{33}(\sigma_1, \sigma_2)$ $k_z(k_x^2 - k_y^2)\lambda_{33}(\sigma_2, -\sigma_1)$ $k_x k_y k_z(k_x^2 - k_y^2)(\lambda_{11} - \lambda_{22})(\sigma_1, \sigma_2)$ $k_z(\lambda_{11} - \lambda_{22})(\sigma_2, -\sigma_1)$ $k_x k_y k_z(\lambda_{11} - \lambda_{22})(\sigma_1, -\sigma_2)$ $k_z(k_x^2 - k_y^2)(\lambda_{11} - \lambda_{22})(\sigma_2, \sigma_1)$ $k_x k_y k_z(k_x^2 - k_y^2)(\lambda_{12} + \lambda_{21})(\sigma_2, -\sigma_1)$ $k_z(\lambda_{12} + \lambda_{21})(\sigma_1, \sigma_2)$ $k_x k_y k_z(\lambda_{12} + \lambda_{21})(\sigma_2, \sigma_1)$ $k_z(k_x^2 - k_y^2)(\lambda_{12} + \lambda_{21})(\sigma_1, -\sigma_2)$ $(k_x, k_y)[(\lambda_{13} - \lambda_{31})\sigma_1 + (\lambda_{23} - \lambda_{32})\sigma_2]$ $(k_y, -k_x)[(\lambda_{13} - \lambda_{31})\sigma_2 - (\lambda_{23} - \lambda_{32})\sigma_1]$ $(k_x, -k_y)[(\lambda_{13} - \lambda_{31})\sigma_1 - (\lambda_{23} - \lambda_{32})\sigma_2]$ $(k_y, k_x)[(\lambda_{13} - \lambda_{31})\sigma_2 + (\lambda_{23} - \lambda_{32})\sigma_1]$

quasinode naturally explains the observed universal thermal conductivity [43,44,47].

Another issue raised by the experiment [33] is the superficial mutual scaling of the in-plane and out-of-plane thermal conductivities, shown as normalized κ_{ab}/T and κ_c/T versus the magnetic field. This was taken as the basis to exclude the horizontal nodal line since the Fermi velocity here is in plane and hence contributes to κ_{ab}/T but not κ_c/T. While it is reasonable in the presence of the horizontal node alone, the argument needs to be re-examined if the vertical node (or quasinode) is also present. In the latter case, both in-plane and out-of-plane thermal transports are possible, and both types of nodes (quasinodes) are subject to the Volovik effect [48], which induces a zero-energy density of states (DOS) $\rho(0) = \mathcal{N}_B \propto \sqrt{B}$, where B is the magnetic field. In the presence of impurity scattering rate γ, the effective DOS is given by $\rho_{\text{eff}}(0) \sim \max(\gamma, \mathcal{N}_B)$. Therefore, when $\mathcal{N}_B > \gamma$, both κ_{ab}/T and κ_c/T are proportional to $\mathcal{N}_B$, which explains the observed mutual scaling.

V. SUMMARY

In this work, we first resolved the paradox between the multicomponent pairings and the uniaxial strain experiments. Then by performing a thorough group classification based on the D_{4h} group with SOC included and by carefully examining different experiments, we concluded that the E_g pairing is the most probable symmetry for Sr_2RuO_4, namely, (d_{xz}, d_{yz}) wave [transforming as $(k_x k_z, k_y k_z)$]. In particular, we pointed out the spin-singlet intraorbital pairings dominated by $(k_x k_z, k_y k_z)\lambda_{(33)}$ and $(k_x k_z, k_y k_z)(\lambda_{(11)} - \lambda_{(22)})$ are compatible with most known experiments.

It is important to ask what pairing mechanism would cause the interlayer E_g pairing, which would possibly also explain why T_c of Sr_2RuO_4 is much lower than that of cuprates. In this regard, a careful study of the three-dimensional three-orbital Hubbard model with SOC may shed light on the underlying pairing mechanism [45,49]. Another remaining question is how to explain the existing phase-sensitive experiments [7–11] and reconcile the singlet nature of the pairing seen in the NMR experiments. This deserves further study, both theoretically and experimentally.

ACKNOWLEDGMENTS

This work is supported by the National Natural Science Foundation of China (under Grants No. 11874205 and No. 11574134) and the National Key Research and Development Program of China (under Grant No. 2016YFA0300401).

APPENDIX A: GROUP CLASSIFICATION

Following the notations in the main text, the pairing matrix can be written as a tensor product $\Lambda_o \otimes \Lambda_s \otimes f_{\mathbf{k}}$, where Λ_o,

Λ_s, and $f_{\mathbf{k}}$ are for the orbital, spin, and momentum, respectively. Λ_o can be expanded on $\lambda_{(ab)}$, and Λ_s can be expanded on σ_μ, where $\lambda_{(ab)}$ denotes the matrix with the (ij)th element given by $\lambda^{ij}_{(ab)} = \delta_{ia}\delta_{jb}$ and σ_0 ($\sigma_{1,2,3}$) represents the spin singlet (triplet). All three parts transform as independent irreducible representations as listed in Table II. After obtaining these representations, we apply the group product to obtain a thorough list of all 148 pairings, as listed in Table III.

APPENDIX B: GAP STRUCTURE

Motivated by the recent NMR [18,19] and neutron [20] experiments, we focus on only the spin-singlet pairings belonging to E_g in this work. We solve the quasiparticle gap with the pairing given by Eq. (4) of the main text. The normal state single-particle Hamiltonian is taken from Refs. [37,39].

First, we studied the gap structure of each isolated case with $d_i = 0.01$ mRy. The results are shown in Fig. 3. For each

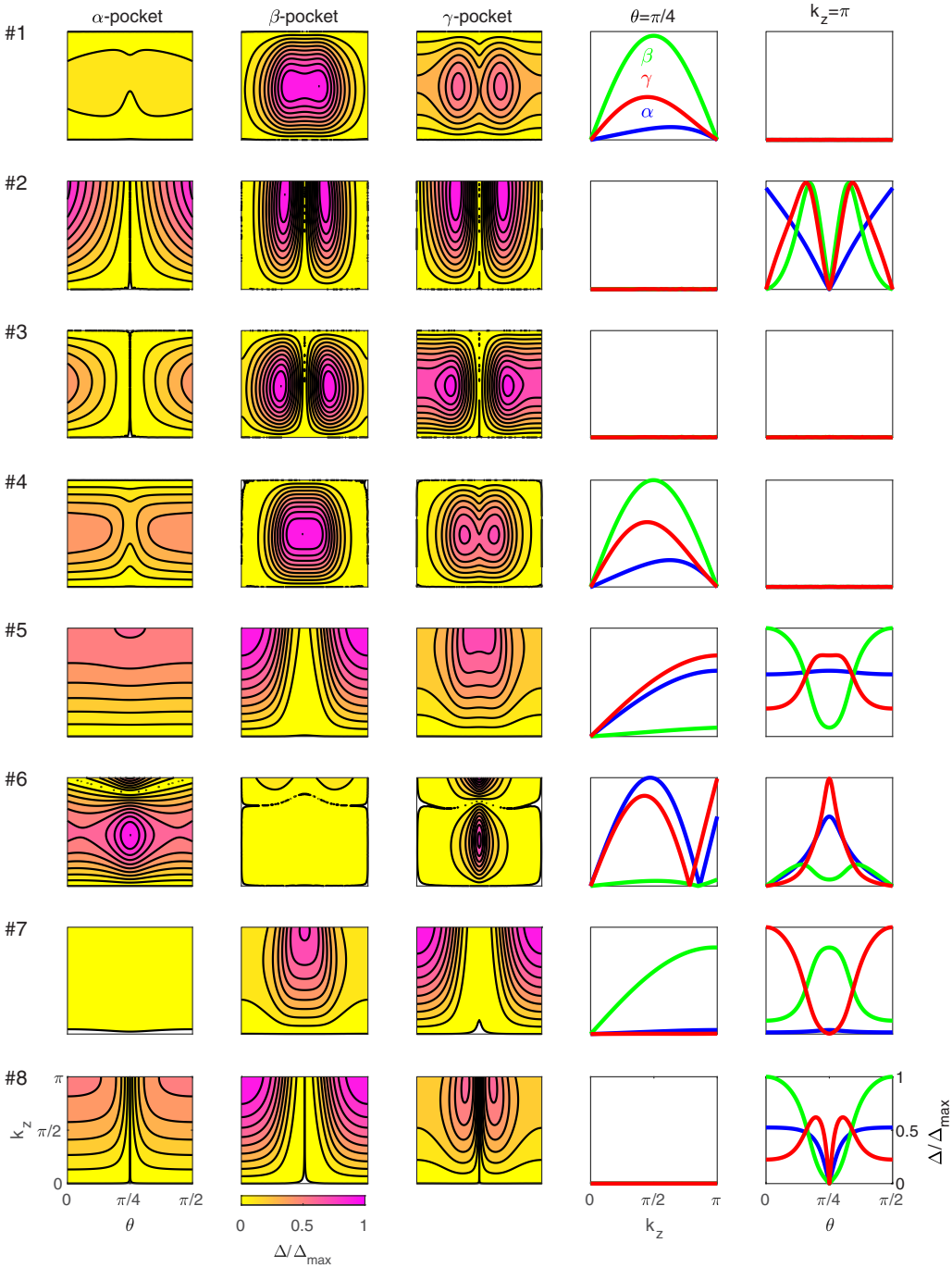

FIG. 3. Gap structures of each spin-singlet pairing belonging to E_g with TR-breaking composition $(d_{xz} + id_{yz})$. The number of each pairing is from the definition in Table I. In calculations, the value of each pairing is chosen to be $d_i = 0.01$ mRy (corresponding to about 0.1 meV). For each pairing (line), the first three panels are color plots of the quasiparticle gap on three Fermi pockets versus the azimuthal angle θ and k_z. In the fourth and fifth panels, the quasiparticle gaps versus k_z (at $\theta = \pi/4$) and θ (at $k_z = \pi$) are plotted explicitly.

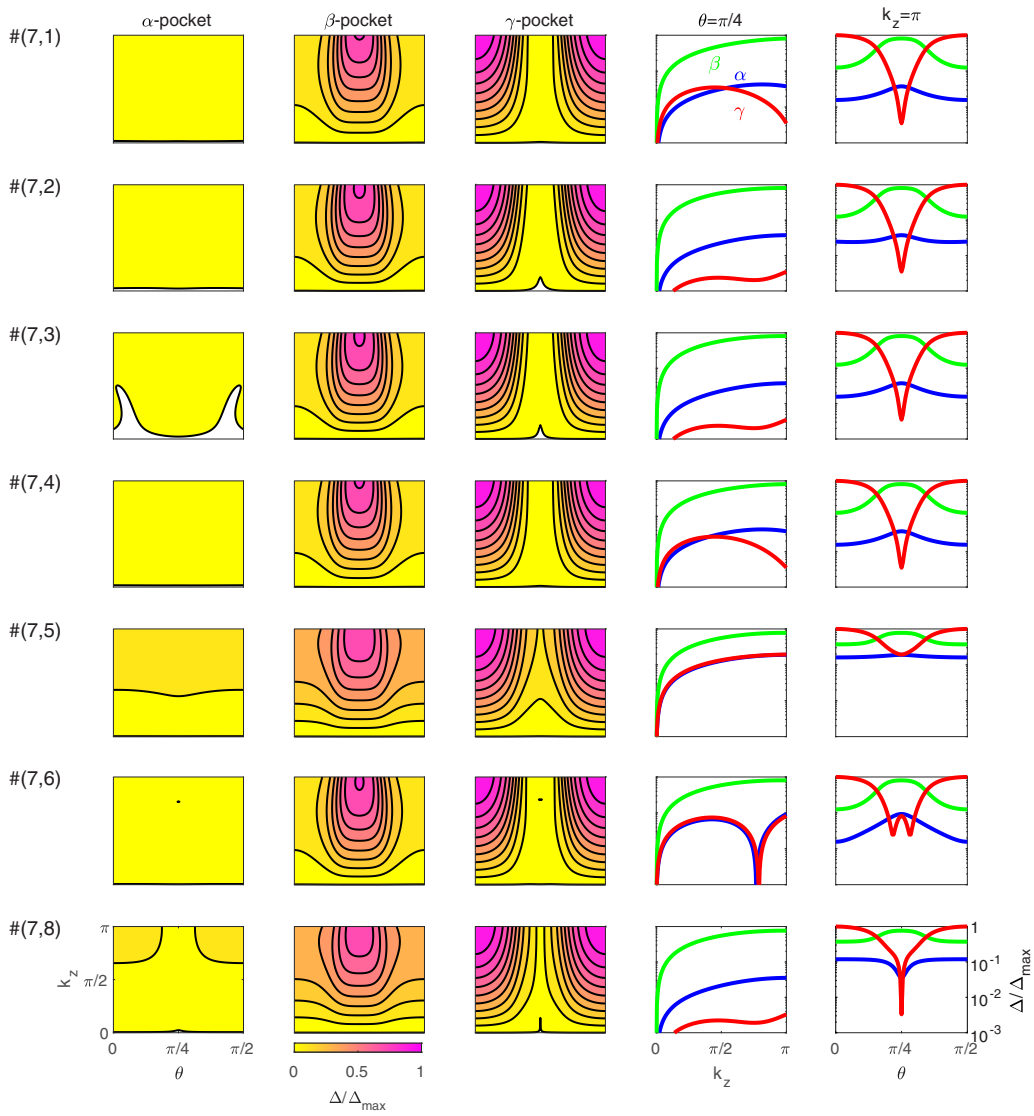

FIG. 4. Gap structures similar to Fig. 3, but with two pairings coexisting. One pairing is chosen to be $d_7 = 0.01$ mRy, and the other is $d_i = d_7/2$. Different from Fig. 3, the last column is plotted with logarithmic scale for clarity.

pairing, the quasiparticle gap amplitude contours on three pockets are shown in the first three columns. In addition, the k_z and θ dependences are explicitly given in the last two columns. In our plots, θ is defined as the azimuthal angle relative to (0,0) for the β and γ pockets, while it is relative to (π, π) for the α pocket. Due to the lattice symmetry, only $0 < \theta < \pi/4$ is presented. From these plots, either horizontal or vertical nodal lines can be found. Moreover, due to the interorbital pairing, an out-of-plane horizontal nodal line with $k_z \neq 0$ is found for pairing 6 ($\lambda_{(12)} + \lambda_{(21)}$).

Next, we study the cases in which two pairings coexist in Fig. 4. We choose $d_7 = 0.01$ mRy, and the other component $d_{i\neq 7} = d_7/2$ for simplicity. Due to the coexistence of two types of pairings, the vertical nodes are eliminated in general. But for the case of (d_7, d_8), the quasinodes remain along the (11) direction and are compatible with the universal thermal conductivity experiments as discussed in the main text. Interestingly, in such a multiorbital pairing with SOC, the gap structure can be very complex. For example, in the case of (d_7, d_2) and (d_7, d_3), we find the original $k_z = 0$ horizontal nodal line is extended to a nodal surface called the Bogoliubov Fermi surface [41]. However, for (d_7, d_6), a nodal point can be found in the α and γ pockets at $\theta = \pi/4$.

[1] Y. Maeno, H. Hashimoto, K. Yoshida, S. Nishizaki, T. Fujita, J. G. Bednorz, and F. Lichtenberg, Nature (London) **372**, 532 (1994).

[2] G. M. Luke, Y. Fudamoto, K. M. Kojima, M. I. Larkin, J. Merrin, B. Nachumi, Y. J. Uemura, Y. Maeno, Z. Q. Mao, Y. Mori, H. Nakamura, and M. Sigrist, Nature (London) **394**, 558 (1998).

[3] V. Grinenko, S. Ghosh, R. Sarkar, J.-C. Orain, A. Nikitin, M. Elender, D. Das, Z. Guguchia, F. Brückner, M. E. Barber, J. Park, N. Kikugawa, D. A. Sokolov, J. S. Bobowski, T. Miyoshi,

Y. Maeno, A. P. Mackenzie, H. Luetkens, C. W. Hicks, and H.-H. Klauss, Nat. Phys., **17** 748 (2021).
[4] J. Xia, Y. Maeno, P. T. Beyersdorf, M. M. Fejer, and A. Kapitulnik, Phys. Rev. Lett. **97**, 167002 (2006).
[5] S. Ghosh, A. Shekhter, F. Jerzembeck, N. Kikugawa, D. A. Sokolov, M. Brando, A. P. Mackenzie, C. W. Hicks, and B. J. Ramshaw, Nat. Phys. **17**, 199 (2020).
[6] S. Benhabib, C. Lupien, I. Paul, L. Berges, M. Dion, M. Nardone, A. Zitouni, Z. Q. Mao, Y. Maeno, A. Georges, L. Taillefer, and C. Proust, Nat. Phys. **17**, 194 (2020).
[7] K. D. Nelson, Z. Q. Mao, Y. Maeno, and Y. Liu, Science **306**, 1151 (2004).
[8] F. Kidwingira, J. D. Strand, D. J. V. Harlingen, and Y. Maeno, Science **314**, 1267 (2006).
[9] J. Jang, D. G. Ferguson, V. Vakaryuk, R. Budakian, S. B. Chung, P. M. Goldbart, and Y. Maeno, Science **331**, 186 (2011).
[10] Y. Yasui, K. Lahabi, M. S. Anwar, Y. Nakamura, S. Yonezawa, T. Terashima, J. Aarts, and Y. Maeno, Phys. Rev. B **96**, 180507(R) (2017).
[11] X. Cai, B. M. Zakrzewski, Y. A. Ying, H.-Y. Kee, M. Sigrist, J. E. Ortmann, W. Sun, Z. Mao, and Y. Liu, arXiv:2010.15800.
[12] T. M. Rice and M. Sigrist, J. Phys.: Condens. Matter **7**, L643 (1995).
[13] A. P. Mackenzie and Y. Maeno, Rev. Mod. Phys. **75**, 657 (2003).
[14] C. W. Hicks, D. O. Brodsky, E. A. Yelland, A. S. Gibbs, J. A. N. Bruin, M. E. Barber, S. D. Edkins, K. Nishimura, S. Yonezawa, Y. Maeno, and A. P. Mackenzie, Science **344**, 283 (2014).
[15] A. Steppke, L. Zhao, M. E. Barber, T. Scaffidi, F. Jerzembeck, H. Rosner, A. S. Gibbs, Y. Maeno, S. H. Simon, A. P. Mackenzie, and C. W. Hicks, Science **355**, eeaf9398 (2017).
[16] M. E. Barber, A. S. Gibbs, Y. Maeno, A. P. Mackenzie, and C. W. Hicks, Phys. Rev. Lett. **120**, 076602 (2018).
[17] C. A. Watson, A. S. Gibbs, A. P. Mackenzie, C. W. Hicks, and K. A. Moler, Phys. Rev. B **98**, 094521 (2018).
[18] A. Pustogow, Y. Luo, A. Chronister, Y.-S. Su, D. A. Sokolov, F. Jerzembeck, A. P. Mackenzie, C. W. Hicks, N. Kikugawa, S. Raghu, E. D. Bauer, and S. E. Brown, Nature (London) **574**, 72 (2019).
[19] A. Chronister, A. Pustogow, N. Kikugawa, D. A. Sokolov, F. Jerzembeck, C. W. Hicks, A. P. Mackenzie, E. D. Bauer, and S. E. Brown, Proc. Natl. Acad. Sci. U.S.A. **118**, e2025313118 (2021).
[20] A. N. Petsch, M. Zhu, M. Enderle, Z. Q. Mao, Y. Maeno, I. I. Mazin, and S. M. Hayden, Phys. Rev. Lett. **125**, 217004 (2020).
[21] A. J. Leggett and Y. Liu, J. Supercond. Novel Magn. **34**, 1647 (2021).
[22] A. Ramires and M. Sigrist, Phys. Rev. B **100**, 104501 (2019).
[23] S.-O. Kaba and D. Sénéchal, Phys. Rev. B **100**, 214507 (2019).
[24] W. Chen and J. An, Phys. Rev. B **102**, 094501 (2020).
[25] W. Huang and H. Yao, Phys. Rev. Lett. **121**, 157002 (2018).
[26] W. Huang, Y. Zhou, and H. Yao, Phys. Rev. B **100**, 134506 (2019).
[27] O. Gingras, R. Nourafkan, A.-M. S. Tremblay, and M. Côté, Phys. Rev. Lett. **123**, 217005 (2019).
[28] S. A. Kivelson, A. C. Yuan, B. Ramshaw, and R. Thomale, npj Quantum Mater. **5**, 43 (2020).
[29] I. Bonalde, B. D. Yanoff, M. B. Salamon, D. J. Van Harlingen, E. M. E. Chia, Z. Q. Mao, and Y. Maeno, Phys. Rev. Lett. **85**, 4775 (2000).
[30] K. Deguchi, Z. Q. Mao, H. Yaguchi, and Y. Maeno, Phys. Rev. Lett. **92**, 047002 (2004).
[31] S. Kittaka, S. Nakamura, T. Sakakibara, N. Kikugawa, T. Terashima, S. Uji, D. A. Sokolov, A. P. Mackenzie, K. Irie, Y. Tsutsumi, K. Suzuki, and K. Machida, J. Phys. Soc. Jpn. **87**, 093703 (2018).
[32] M. Suzuki, M. A. Tanatar, N. Kikugawa, Z. Q. Mao, Y. Maeno, and T. Ishiguro, Phys. Rev. Lett. **88**, 227004 (2002).
[33] E. Hassinger, P. Bourgeois-Hope, H. Taniguchi, S. René de Cotret, G. Grissonnanche, M. S. Anwar, Y. Maeno, N. Doiron-Leyraud, and L. Taillefer, Phys. Rev. X **7**, 011032 (2017).
[34] M. H. Fischer and E. Berg, Phys. Rev. B **93**, 054501 (2016).
[35] R. Willa, Phys. Rev. B **102**, 180503(R) (2020).
[36] Y. Yu and S. Raghu, Phys. Rev. B **100**, 094517 (2019).
[37] C. N. Veenstra, Z.-H. Zhu, M. Raichle, B. M. Ludbrook, A. Nicolaou, B. Slomski, G. Landolt, S. Kittaka, Y. Maeno, J. H. Dil, I. S. Elfimov, M. W. Haverkort, and A. Damascelli, Phys. Rev. Lett. **112**, 127002 (2014).
[38] A. Tamai, M. Zingl, E. Rozbicki, E. Cappelli, S. Riccò, A. de la Torre, S. McKeown Walker, F. Y. Bruno, P. D. C. King, W. Meevasana, M. Shi, M. Radović, N. C. Plumb, A. S. Gibbs, A. P. Mackenzie, C. Berthod, H. U. R. Strand, M. Kim, A. Georges, and F. Baumberger, Phys. Rev. X **9**, 021048 (2019).
[39] E. Pavarini and I. I. Mazin, Phys. Rev. B **74**, 035115 (2006).
[40] K. Iida, M. Kofu, K. Suzuki, N. Murai, S. Ohira-Kawamura, R. Kajimoto, Y. Inamura, M. Ishikado, S. Hasegawa, T. Masuda, Y. Yoshida, K. Kakurai, K. Machida, and S. Lee, J. Phys. Soc. Jpn. **89**, 053702 (2020).
[41] D. F. Agterberg, P. M. R. Brydon, and C. Timm, Phys. Rev. Lett. **118**, 127001 (2017).
[42] A. C. Durst and P. A. Lee, Phys. Rev. B **62**, 1270 (2000).
[43] H. Meng, H. Zhang, W.-S. Wang, and Q.-H. Wang, Chin. Phys. Lett. **35**, 127402 (2018).
[44] W.-S. Wang, C.-C. Zhang, F.-C. Zhang, and Q.-H. Wang, Phys. Rev. Lett. **122**, 027002 (2019).
[45] H. G. Suh, H. Menke, P. M. R. Brydon, C. Timm, A. Ramires, and D. F. Agterberg, Phys. Rev. Res. **2**, 032023 (R) (2020).
[46] R. Sharma, S. D. Edkins, Z. Wang, A. Kostin, C. Sow, Y. Maeno, A. P. Mackenzie, J. C. S. Davis, and V. Madhavan, Proc. Natl. Acad. Sci. USA **117**, 5222 (2020).
[47] J. F. Dodaro, Z. Wang, and C. Kallin, Phys. Rev. B **98**, 214520 (2018).
[48] G. E. Volovik, JETP Lett. **58**, 457 (1993).
[49] H. S. Røising, T. Scaffidi, F. Flicker, G. F. Lange, and S. H. Simon, Phys. Rev. Res. **1**, 033108 (2019).